Journal of ELECTRONIC MATERIALS
DOI: 10.1007/s11664-016-5010-7

Diamond and Carbon Nanotube Composites for Supercapacitor Devices

JOÃO VITOR SILVA MOREIRA,[1] PAUL WILLIAM MAY,[2] EVALDO JOSÉ CORAT,[3] ALFREDO CARLOS PETERLEVITZ,[4] ROMÁRIO ARAÚJO PINHEIRO,[3] and HUDSON ZANIN[1,4,5,6]

1.—Laboratory of Energy Storage and Supply, Universidade do Vale do Paraiba, Av. Shishima Hifumi 2911, Sao Jose dos Campos, SP CEP: 12244-000, Brazil. 2.—School of Chemistry, University of Bristol, Bristol BS8 1TS, UK. 3.—National Institute for Space Research, Av. dos Astronautas 1758, Sao Jose dos Campos, SP CEP: 12227-010, Brazil. 4.—Carbon Sci-Tech Labs, University of Campinas, Campinas 13081-970, Brazil. 5.—e-mail: hudsonzanin@gmail.com. 6.—e-mail: hudson@fee.unicamp.br

We report on the synthesis and electrochemical properties of diamond grown onto vertically aligned carbon nanotubes with high surface areas as a template, resulting in a composite material exhibiting high double-layer capacitance as well as low electrochemical impedance electrodes suitable for applications as supercapacitor devices. We contrast results from devices fabricated with samples which differ in both their initial substrates (Si and Ti) and their final diamond coatings, such as boron-doped diamond and diamond-like carbon (DLC). We present for first time a conducting model for non-doped DLC thin-films. All samples were characterized by scanning and transmission electron microscopy and Fourier transform infrared and Raman spectroscopy. Our results show specific capacitance as high as 8.25 F g^{-1} (~1 F cm^{-2}) and gravimetric specific energy and power as high as 0.7 W h kg^{-1} and 176.4 W kg^{-1}, respectively, which suggest that these diamond/carbon nanotube composite electrodes are excellent candidates for supercapacitor fabrication.

Key words: Diamond, carbon, supercapacitor, electrochemical cell, nanotube

INTRODUCTION

The worldwide increase in use of portable and wearable electronic devices is driving research into low-cost, flexible, light-weight, and environmentally friendly energy storage and supply devices. An example is supercapacitors, which bridge the gap between rechargeable batteries and conventional high-power electrostatic capacitors.[1] Carbon electrodes are very attractive candidates for supercapacitor device fabrication, especially if the electrodes have a three-dimensional (3D) interconnected porous texture facilitating ion transport by providing a smaller resistance and shorter diffusion pathways.[2] 3D carbon-microstructured electrodes use ion adsorption on the highly porous surface to store charge, where electrons in each electrode and ions in the electrolyte form a double-layer (DL) capacitor.[3–5] Consequently, it is desirable to fabricate a high surface area in a highly conductive material, preferably one which has high chemical stability in different acid and basic media. Among carbon materials, which are commonly used in electrode storage devices, carbon nanotubes (CNTs) and diamond have some advantages. Boron-doped diamond (BDD) and diamond-like carbon (DLC) electrodes are known as highly chemical stable materials with a wide electrochemical potential window; however, they often suffer from very low background current and high electrochemical impedance. To overcome these limitations, metallic conductivity multi-walled carbon nanotubes (MWCNTs) can be prepared so that they are vertically aligned to the substrate forming a highly porous electrode. Composite electrodes made

(Received June 14, 2016; accepted September 28, 2016)

Published online: 21 October 2016

by coating 'forests' of these vertically aligned MWCNTs (VAMWCNTs) with BDD deposited using chemical vapor deposition (CVD) have been reported by our group and others, and found to be superb electrodes for electrochemical sensors (with high sensitivity and extremely high capacitance values)[6] and field emission devices with exceptionally long lifetimes. The main electrochemical advantages are that these composite materials allow current to be drained from the diamond surface down to the charge collectors with very low potential barrier at the junction.[6,7] Additionally, the DL capacitance of these systems can be adjusted by varying the length of the CNTs without affecting the electrode total resistance.[6,7] These morphological properties are expected to facilitate rapid charge/discharge kinetics, providing both high gravimetric specific energy and power in compact, highly conductive, carbon electrodes.[8]

Until now, literature reports have been limited to high-surface-area diamond electrodes for supercapacitors. Gao and Nebel[9] described increasing the area of BDD electrodes using a top-down plasma-etching method. These electrodes showed a capacitance of 0.69 mF cm^{-2} in aqueous solution. Hérbert et al.[4] reported on porous diamond thin films with high DL capacitance up to 3 mF cm^{-2} as well as low electrochemical impedance for supercapacitors devices. In their electrodes, BDD was grown on a highly porous polypyrrole scaffold prepared by CVD. In a different report, they combined aligned MWCNTs with BDD producing a high-surface-area electrode with DL capacitance values up to 1 mF cm^{-2}.[7]

In various recent reports[6,10,11] our group has demonstrated both BDD and DLC high-surface-area electrodes grown on VACNTs with interfacial capacitance values ~0.6 mF cm^{-2}, as well as low charge-transfer impedance in the presence of a redox probe using a standard three-electrode system. The ensemble of experimental results suggests that the enhanced electrochemical responses are not simply due to areas in which the CNT support is exposed to the electrolyte solution, but instead from the increased electrode active area. In this work, we study for the first time the electrochemical performance of high-surface-area diamond–VACNT composite electrodes in a functioning supercapacitor set-up. An important component of a supercapacitor is the electrolyte, and we chose to use a thin solid electrolyte composed of a mixture of polyvinyl alcohol (PVA) and phosphoric acid (H_3PO_4) because it is easier to handle than aqueous electrolytes, avoiding leaking and cell malfunction.

EXPERIMENTAL

Chemicals and Solutions

PVA and phosphoric acid were purchased from Sigma-Aldrich. The thin solid electrolyte was prepared with PVA 10% in deionized water at 90°C, and 8% volume of the solution was diluted in concentrated phosphoric acid (H_3PO_4/PVA/H_2O) all in a beaker.[1] After preparation, the electrolyte takes the form of a gel, which was then spread as a μm-thin layer (~0.1 mg) onto the electrode surfaces.

Materials Preparation

VACNT Film Growth

VACNT films were produced using a microwave plasma CVD chamber operating at 2.45 GHz.[12] Substrates were Si or Ti (5 mm × 5 mm) covered with a 10-nm Ni layer deposited by electron-beam evaporation. The Ni layer was heated from 350°C to 800°C over a period of 5 min in a N_2/H_2 (10/90 sccm) plasma, inducing the formation of nanoparticles which promote the CNT growth. VACNT growth was initiated by introducing CH_4 (14 sccm) into the chamber for 1 min, maintaining a substrate temperature of 800°C and a reactor pressure of 30 torr. After growth, the samples, now coated in a 'forest' of VACNTs, were placed into a plasma-enhanced CVD (PECVD) reactor (~400 V, pulse frequency 20 kHz) with an oxygen flow rate of 1 sccm at a pressure of 5 mtorr for 1 min. This was done in order to improve wettability and create oxygen functional groups on the VACNT surfaces.[13]

BDD Film Growth

The VACNT samples were then electrospray-seeded with a suspension of 5-nm detonation nanodiamond in methanol, which caused the CNTs to form microstructures with their tips joined together, producing 3D microstructures resembling teepees, honeycomb or ridge structures.[6] In this work, the 'crest' of each ridge consisted of ~10–1000 CNTs joined at their sides and tips, with an areal density of ~10^7 cm^{-2}. Subsequent (0.5 h and 1 h, for contrast) diamond CVD was performed in a hot filament reactor using 1% CH_4/H_2 with diborane (B_2H_6) as a source of boron, causing the microstructure to become coated with a thin (0.25–0.5 μm) layer of BDD connected crystals. The gas-phase B concentration was sufficient to ensure that the diamond coating was heavily doped and therefore had near-metallic conductivity.[6]

DLC Film Growth

DLC layers were deposited using a PECVD reactor fed with hexane vapor and argon gas at 130–400 Pa, and a discharge voltage of −700 V at a pulse frequency of 20 kHz. For preparation of the composite VACNT/DLC samples, the previously prepared VACNT forest samples were used as substrates. Before growth, *n*-hexane was sprayed onto the samples, and then the plasma was struck under argon and *n*-hexane vapor for ~10 min.[10,14] This deposited DLC over the substrate to a thickness range from 2 nm to 20 nm. Following this

procedure, the DLC film on VACNT, I_D/I_G = 0.52, which corresponds to ~45–55% sp^3 carbon and Tauc band gap ~1.6–1.8 eV (see Fig. 2a).[15]

Materials Characterization

A JEOL6330F and FEI-Inspect F50 field emission scanning electron microscope (SEM) were used to evaluate structural arrangements and monitor details on the surface morphology. Raman spectroscopy (Renishaw Invia) with ultraviolet 325-nm laser excitation was used to analyze the structural changes on the samples. Curve fitting and data analysis software (Fityk) was used to assign the peak locations and fitting of all spectra. Some samples were further characterized by transmission electron microscopy (TEM) (JEOL 3010) adjusted to 300 kV and 120 μA using a LaB_6 filament. For TEM images, the samples were pulverised by hand in a pestle, dispersed in ethanol, and then drop-cast onto a copper mesh coated with carbon film.

Electrochemical Set-Up

Electrochemical Cell

The electrochemical supercapacitor cell used in this work was a custom-built cell composed of polyacrylate, a hard, low-cost polymer (shown in red in Fig. 1) used for sample encapsulation, and AISI304 stainless steel (shown in green) collectors, to which the electric contacts were made. The cell was designed to be easy to handle and simple to exchange samples, electrolyte and separators.

Electrochemical Assays

Two identical electrodes, composed of either the VACNT-diamond ridges or the diamond-DLC structures, were coated with the thin solid electrolyte and placed in contact with each other in parallel.[16] These formed the working electrode and counter electrode, and they were separated by thin paper foil as a mesoporous membrane all inside the electrochemical supercapacitor cell, consolidating a device controlled by an Autolab PGSTAT302 N.

The devices were characterised by cyclic voltammetry (CV) and galvanostatic charge–discharge (g-C/D) in a two-electrode cell set-up. The CV measurements were carried out from 1 mV s^{-1} to 1000 mV s^{-1} and between 0 V and 1.0 V. The g-C/D measurements were performed between 0 V and 1.0 V using different electric currents.

RESULTS AND DISCUSSION

Materials Characterization

UV Raman spectra of the porous diamond samples were deconvoluted and are presented in Fig. 2.

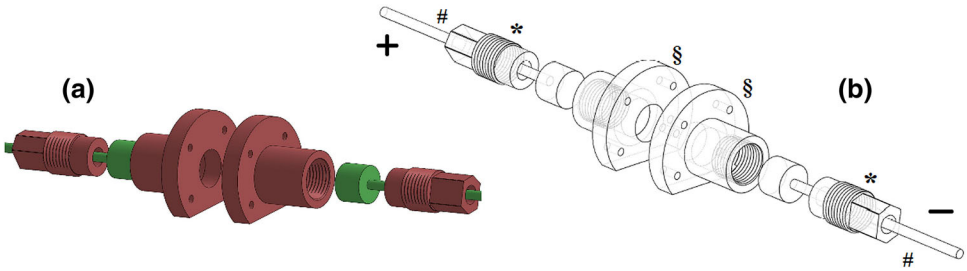

Fig. 1. Representation of the electrochemical supercapacitor cell (a) solid and (b) transparent views, where # represent stainless steel for electric contact, § the case for the electrode, electrolyte and membrane encapsulation, and * sealing components.

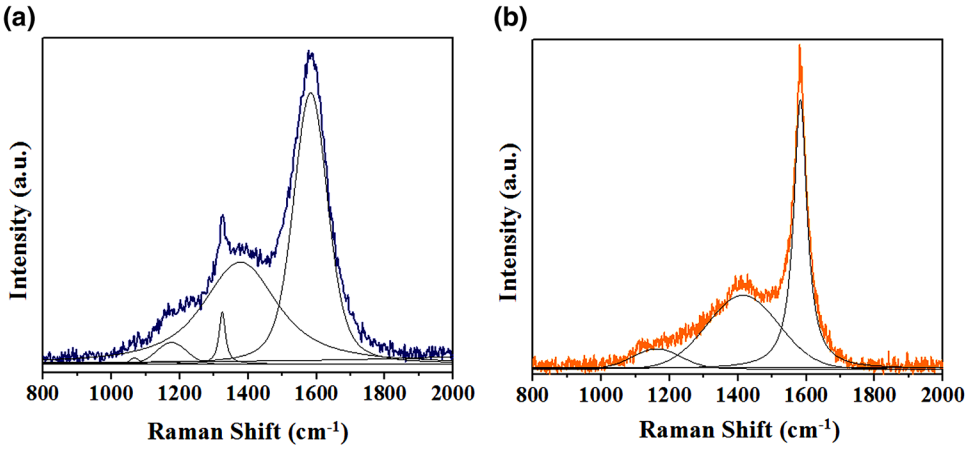

Fig. 2. Laser Raman spectra of porous (a) BDD and (b) DLC electrodes using 325-nm laser excitation. The spectra have been deconvoluted for band and peak identification.

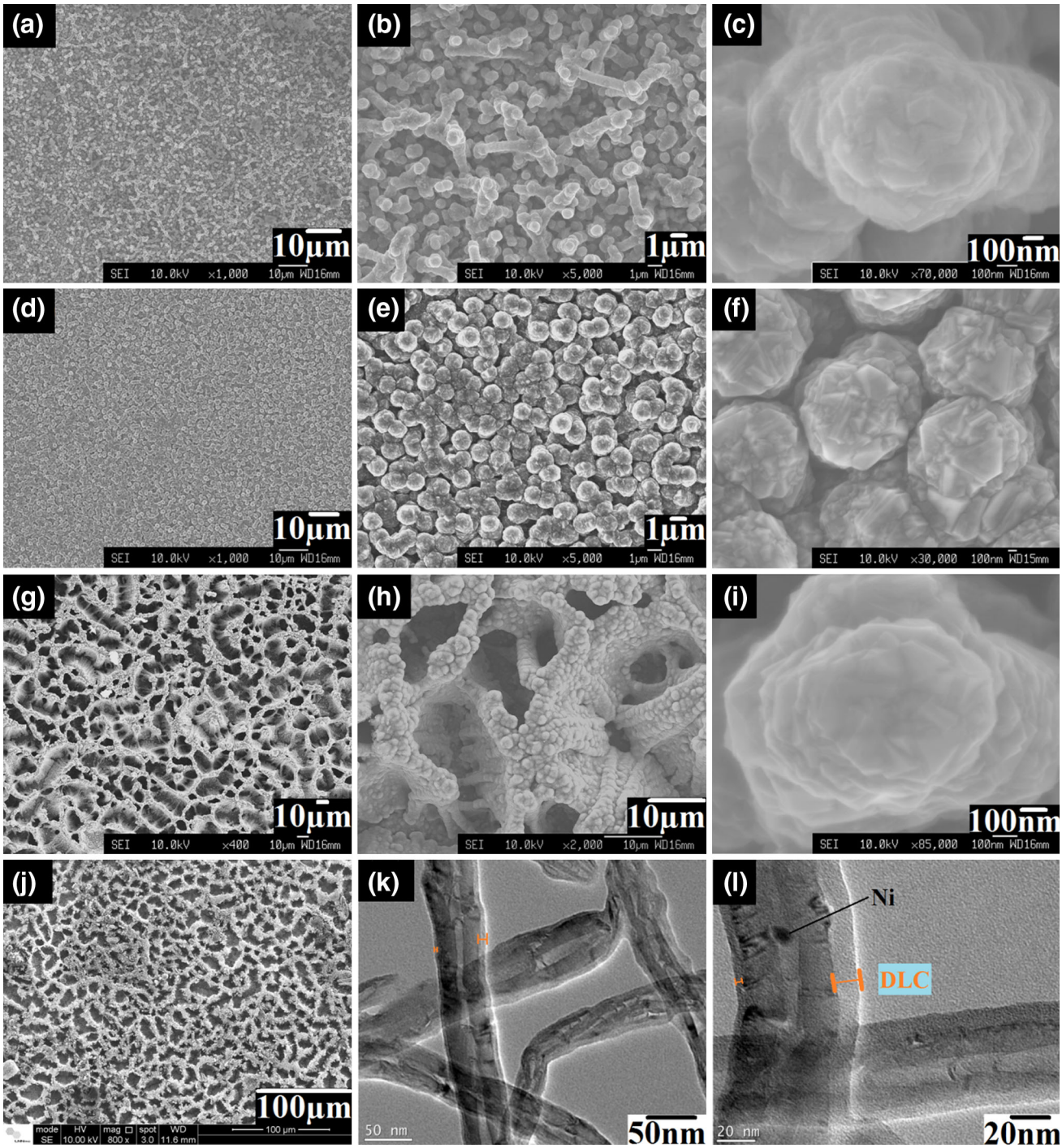

Fig. 3. SEM images of (a–c) Si/VACNT/BDD grown for 0.5 h, (d–f) Si/VACNT/BDD grown for 1 h, (g–i) Ti/VACNT/BDD grown for 0.5 h and (j) Ti/VACNT/DLC. (k, l) TEM images of DLC-covered MWCNT.

In Fig. 2a, a sharp diamond peak (1328 cm^{-1}) and two main bands D (~1360 cm^{-1}) and G (~1582 cm^{-1}) are used for deconvolution. The wide Raman peak in the vicinity of 1328 cm^{-1} is the characteristic peak of sp^3 nanodiamond, with the offset from the usual value of 1332 cm^{-1} probably due to the Fano distortion arising from the high B doping levels. The D band is associated with a double-resonance process involving a phonon and a defect, commonly observed in disordered nanoscale carbon phases.[17] This observation is consistent with the SEM images (Fig. 3) showing large amounts of edges and boundaries present in the film. The G-band stems from in-plane vibrations and has E_{2g}

symmetry corresponding to stretching vibrations in the basal plane (sp^2 domains) of graphene from carbon nanotube scaffolds. In Fig. 2a, two additional bands were found to be necessary for accurate fitting, at ~1060 cm^{-1} and ~1180 cm^{-1}. The small band at around 1060 cm^{-1} (T-peak) corresponds to the peak in the CC sp^3 vibration density of states[18] usually detected by UV excitation. The band centered at 1180 cm^{-1} is assigned to disordered carbon and transpolyacetylene present at the grain boundaries, which is often prominent in nanophase diamond samples.[19]

A UV Raman spectrum of VACNT/DLC is presented in Fig. 2b. For spectrum deconvolution, fitting used the typical values for the D (~1400 cm^{-1}) and G (~1580 cm^{-1}) DLC bands. Both bands are a combination of D and G from the DLC and CNTs.[17–20] Additionally, we found it necessary to include the peak at 1150 cm^{-1}, which is assigned to disordered carbon at the grain boundaries area.

Figure 3 shows SEM (a–j) and TEM images (k, l) of (a–f) Si/VACNT/BDD, (g–i) Ti/VACNT/BDD and (j–l) Ti/VACNT/DLC samples. Figure 3a–f contrasts BDD grown onto Si/VACNT for (a–c) 0.5 h and (d–f) 1 h, suggesting that longer diamond deposition time leads to both larger grain size and a continuous film, instead of the desired porous one. These microstructures patterned from Fig. 3a–f consist of ~10–20 CNTs joined at the top covered by 0.25–0.5 μm thickness of BDD. Although it has smaller pore size (a few microns), the BDD sample grown for 1 h on Si/VACNT still allows ions to penetrate easily (perhaps because the anions used are much smaller than the pore size).

Figure 3g–i shows SEM images from BDD grown for 0.5 h on Ti/VACNT. Larger pore sizes (~10 μm) are produced compared to those in the Si/VACNT/BDD samples (~1 μm). The microstructure patterned in Fig. 3g and h consists of ~500–1500 CNTs joined at the top, covered by ~0.25 μm thickness of BDD. The exactly thickness could not be measured due to the crystalline nature of CVD diamond, which obscured the CNT walls.

Figure 3j shows an SEM image from DLC grown for 10 min on Ti/VACNT, in a similar procedure to our previous work.[10,11,14] This microstructure is comparable to that observed from Ti/VACNT/BDD, which shows that the wetting/seeding process caused the CNTs to clump into teepees, ridges or honeycomb depending on the density of the VACNT forest, while CVD growth coated them with a thin diamond film. Figure 3k and l shows TEM micrographs of crystalline bamboo-like structures with diameters ranging from 20 nm to 40 nm that are covered by DLC thin films. The nanotubes have an interplanar spacing of ~0.33 ± 0.02 nm and encapsulate small catalytic nickel precursor particles (Fig. 3l). The DLC thin film thickness varies along the tubes from 2 nm to 20 nm, which is an important result that suggests a reason why porous DLC films conduct electricity while conventional undoped DLC films do not. Such thin-solid films with nanosize thickness present a very small volume:surface ratio, which leads to a high concentration of defects at the surface, due to dangling bonds. Considering the bond lengths of sp^3–sp^3, sp^3–sp^2 and sp^2–sp^2 carbon are all ~0.15 nm (only an order of magnitude smaller than some thin film thickness),[20,21] and graphite and diamond interplanar spaces are about 0.35 nm and 0.44 nm, respectively, one could expect that those films may act like a quantum barrier to electrons crossing through and have many solitons at the surfaces and interfaces.[22] Such a barrier could offer extra impedance to electrons to propagate through the film, but nevertheless still allow them to cross. Moreover, such high-energy surface solitons could exhibit stable propagation at many surfaces and interfaces conducting charge.[23]

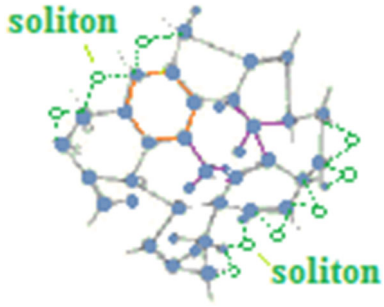

Fig. 4. Schematic representation of few atoms thick of sp^2 and sp^3 carbon hybridization of DLC, which indicate soliton formation at the surface.

Figure 4 illustrates a simplified picture regarding this soliton model. To explain that better, we start from the DLC definition, which is a class of amorphous carbon material that displays some of the typical properties of diamond. From quantum theory, DLC is a combination of sp^3 (tetrahedral diamond bonds) and sp^2 (trigonal graphite bonds) orbitals arranged in such way that, in very thin films, many dangling bonds remain throughout the film and at surfaces/interfaces. To minimize the local energy, the dangling bonds join to their near neighbors in such way that a travelling wave (a soliton) forms at the surface. Because of the relatively high concentration of these solitons, electrons are free to move on the surface and through the film. It is likely that as a result new energy levels, such as trap states, are formed in the band gap, into which electrons can be readily promoted, increasing the conductivity. This model is undoubtedly very speculative but helps explain the electrochemical behavior of DLC electrodes. A detailed photoelectrochemical study is underway to provide evidence for this model.

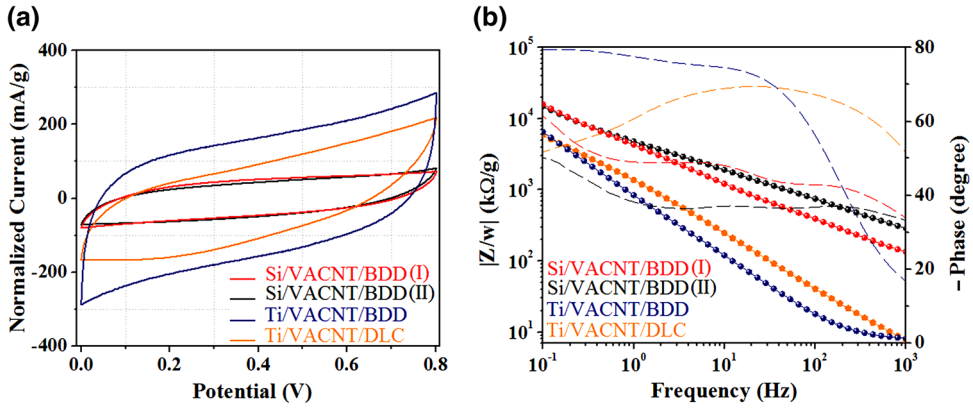

Fig. 5. (a) Cyclic voltammograms at 100 mV s^{-1} and (b) Bode plots (the magnitude of the impedance, |Z| normalized by weight, plotted against frequency) and the phase measured from supercapacitor devices (Color figure online).

Table I. Specific capacitance, energy and power from porous diamond supercapacitor devices

	Si/VACNT/ BDD (I): 0.5 h	Si/VACNT/ BDD (II): 1 h	Ti/VACNT/BDD	Ti/VACNT/DLC
Specific capacitance (F g^{-1})	2.7 ± 0.1	2.2 ± 0.2	8.3 ± 0.5	4.4 ± 0.3
Specific capacitance (mF cm^{-2})	0.5 ± 0.1	0.4 ± 0.1	1.1 ± 0.3	0.9 ± 0.2
Charge efficiency (%)	35.4 ± 0.2	49.4 ± 0.2	74.1 ± 0.3	34.2 ± 0.2
Gravimetric specific energy (W h kg^{-1})	0.24 ± 0.04	0.19 ± 0.04	0.70 ± 0.25	0.40 ± 0.06
Gravimetric specific power (W kg^{-1})	126.40 ± 0.04	48.40 ± 0.04	176.4 ± 0.3	58.8 ± 0.1

Electrochemical Behavior

Figure 5a and c shows the electrochemical data from porous diamond electrodes in the electrochemical supercapacitor cell (Fig. 1). Those voltammograms have a "quasi-rectangular" shape, which is typical of interfacial DL charging in a non-Faradaic process. Normalized capacitance by weight and area both extracted from Fig. 5a and b are presented in Table I. CV measurements from 1 mV s^{-1} to 1000 mV s^{-1} confirmed that the specific capacitance (SC) values are constant for low scan rates and correspond to the capacitance under equilibrium conditions. These SC values determined from CVs at 100 mV s^{-1} are very similar to the values obtained from discharging measurements.

Table I shows SC, gravimetric specific energy, and power from porous diamond electrodes in supercapacitor devices under similar operation conditions. Comparing Fig. 5 and Table I, one can say that longer CVD diamond deposition times are not beneficial for device capacitance, because of the slight increase in impedance (compare the black and red dotted lines in Fig. 5b) and reduced capacitance (compare the black and red dotted lines in the CVs in Fig. 5a and the SEM images in Fig. 3a and d). Although DLC electrodes showed high performance, BDD diamond on Ti/VACNT is our best candidate for supercapacitor device fabrication with higher SC, charge efficiency, gravimetric specific energy, and power.

CONCLUSION

We have presented an electrochemical DL capacitor prepared from a new class of porous diamond. Contrasting materials in a supercapacitor device, the Ti/VACNT/BDD electrode showed higher SC, charge efficiency, gravimetric specific energy, and power than other porous diamond electrodes, probably due to better electron and ion transport during the charge–discharge processes. We are currently studying the pseudocapacitance characteristics of these supercapacitors which involves investigating different electrode terminations for Li ion intercalation and for polymer bonding. These supercapacitors could be a solution to the mismatch between the fast growth in power required by devices and the inability of batteries to discharge efficiently at high rates. Energy storage and supply devices, such these supercapacitors, could bridge the gap between rechargeable batteries and conventional high-power electrostatic-capacitor devices. This is because they occupy a region between batteries and dielectric capacitors on the Ragone plot,[24] which describes the relationship between gravimetric specific energy and power.

ACKNOWLEDGEMENTS

We would like to thank the LME/LNLS-Campinas and the University of Bristol for microscope facilities and NANOBIO for the Autolab facility. Also, we gratefully acknowledge the Brazilian Agency Fapesp

(2014/02163-7) and the Royal Society for Newton Travel Fund NI140181 for financial support.

REFERENCES

1. D. Ge, L. Yang, L. Fan, C. Zhang, X. Xiao, Y. Gogotsi, and S. Yang, *Nano Energy* 11, 568 (2015).
2. D.W. Wang, F. Li, M. Liu, G.Q. Lu, and H.M. Cheng, *Angew. Chem. Int. Ed.* 48, 1525 (2009).
3. J. Chmiola, G. Yushin, Y. Gogotsi, C. Portet, P. Simon, and P.L. Taberna, *Science* 313, 1760 (2006).
4. C. Hebert, E. Scorsone, M. Mermoux, and P. Bergonzo, *Carbon* 90, 102 (2015).
5. B.C. Lourencao, T.A. Silva, H. Zanin, P.W. May, E.J. Corat, O. Fatibello-Filho, *J. Solid State Electrochem* 20, 2403 (2016).
6. H. Zanin, P.W. May, D.J. Fermin, D. Plana, S.M.C. Vieira, W.I. Milne, E.J. Corat, and A.C.S. Appl, *Mater. Interfaces* 6, 990 (2014).
7. C. Hebert, J.P. Mazellier, E. Scorsone, M. Mermoux, and P. Bergonzo, *Carbon* 71, 27 (2014).
8. J.-H. Kim, K. Zhu, Y. Yan, C.L. Perkins, and A.J. Frank, *Nano Lett.* 10, 4099 (2010).
9. F. Gao, C.E. Nebel, ACS *Appl Mater. Interfaces* (2015). doi: 10.1021/acsami.5b07027.
10. H. Zanin, P.W. May, R.L. Harniman, T. Risbridger, E.J. Corat, and D.J. Fermin, *Carbon* 82, 288 (2015).
11. T.A. Silva, H. Zanin, P.W. May, E.J. Corat, and O. Fatibello-Filho, *ACS Appl. Mater. Interfaces* 6, 21086 (2014).
12. H. Zanin, C.M.R. Rosa, N. Eliaz, P.W. May, F.R. Marciano, and A.O. Lobo, *Nanoscale* 7, 10218 (2015).
13. M.M. Zogbi, E. Saito, H. Zanin, F.R. Marciano, and A.O. Lobo, *Mater. Lett.* 132, 70 (2014).
14. H. Zanin, P.W. May, M.H.M.O. Hamanaka, E.J. Corat, and A.C.S. Appl, *Mater. Interfaces* 5, 12238 (2013).
15. H. Zanin, P.W. May, A.O. Lobo, E. Saito, J.P.B. Machado, G. Martins, V.J. Trava-Airoldi, and E.J. Corat, *J. Electrochem. Soc.* 161, H1 (2014).
16. Y. Li, K. Sheng, W. Yuan, and G. Shi, *Chem. Commun.* 49, 291 (2013).
17. V. Carozo, C.M. Almeida, E.H.M. Ferreira, L.G. Cancado, C.A. Achete, and A. Jorio, *Nano Lett.* 11, 4527 (2011).
18. J.V.S. Moreira, E.J. Corat, P.W. May, L.D.R. Cardoso, P.A. Lelis, H. Zanin, *J. Electron. Mater.* 45, 5781 (2016).
19. D. Pradhan, Y.C. Lee, C.W. Pao, W.F. Pong, and I.N. Lin, *Diam. Rel. Mater.* 15, 2001 (2006).
20. James, *Sigma Bonds Come in Six Varieties: Pi Bonds Come in One* (2010), http://www.masterorganicchemistry.com/2010/10/13/sigma-bonds-come-in-six-varieties-pi-bonds-come-inone/. Accessed 13 Oct 2016.
21. D. Srivastava, M. Menon, and K.J. Cho, *Phys. Rev. Lett.* 83, 2973 (1999).
22. W.H. Chen, Y.J. He, and H.Z. Wang, *Opt. Express* 14, 11271 (2006).
23. H.Y. Choi and E.J. Mele, *Phys. Rev. B* 34, 8750 (1986).
24. L.L. Zhang and X.S. Zhao, *Chem. Soc. Rev.* 38, 2520 (2009).